Dynamics of self-assembly of flower-shaped magnetic colloidal clusters

A. Ray, S. Aliaskarisohi, and T. M. Fischer*
Institute of Physics, Universität Bayreuth, Bayreuth 95440, Germany
(Received 11 May 2010; published 24 September 2010)

In a static magnetic field paramagnetic and nonmagnetic colloids immersed in a ferrofluid self-assemble into fluctuating colloidal flowers. Adsorption and desorption of nonmagnetic petals to larger paramagnetic cores and changes in the petal conformation around the paramagnetic core induce a fluctuating dynamics. We track the motion of colloidal petals on the paramagnetic core. Adsorption and desorption of petals occur on a larger time scale than the rotational diffusion of the petals. Magnetic dipole interactions split the motion of the petals into different modes of rotational diffusion. Modes of rotational diffusion that change the petal conformation are suppressed compared to the conformation invariant rotational diffusion of all petals. The suppression of higher modes of rotational diffusion results in a subdiffusive dynamics of the individual petals.

DOI: 10.1103/PhysRevE.82.031406 PACS number(s): 82.70.Dd

I. INTRODUCTION

Colloidal assemblies are mesoscopic systems in thermodynamic equilibrium. Understanding the complex structures of these assemblies, the soft interactions between the individual particles, and the resultant dynamics in real space is of current interest; because colloidal assemblies are being used as models for atomic crystals [1] for glasses [2], for van der Waals crystals [3], and as systems for the study of dynamic self-assembly [4,5]. The softness of the interactions gives rise to fluctuations around the equilibrium that allows observing directly the transport processes [6–8] which lead to the dynamic self-assembly of the system. Diffusion is considered as one of these basic passive means for irreversible transport into equilibrium. It arises from fluctuations of the particle velocity due to stochastic forces. These forces act on the diffusing particles due to collisions with other particles from a reservoir at a certain temperature. In the presence of stochastic and deterministic microscopic forces, macroscopic diffusion can be expressed as the zeroth moment of the particle velocity autocorrelation and/or cross-correlation functions [9]. Kubo [9] extended a generalized concept of diffusion that allows defining and measuring the diffusion of interacting particles. It has been shown by Erb *et al.* [5] that paramagnetic and nonmagnetic colloidal particles immersed in a ferrofluid can self-assemble into colloidal flowers in a static magnetic field. The colloidal flowers result from the effective dipolar attraction of the paramagnetic colloids in which nonmagnetic particles behave as magnetic holes in the ferrofluidic background. The dipole interaction is a tensorial traceless interaction that depends on the angle between the magnetic moments and the particle separation. For holes sitting at the pole positions above or below the paramagnetic bead the dipole interaction with the paramagnetic bead is repulsive. In the equatorial plane on the other hand it is attractive. The dipole interaction between two magnetic holes on the other hand is repulsive in the plane normal to the magnetic moments and attractive along the direction of the magnetic moments. The planar structure of the colloidal flowers is a result of the complex angular dependency of the dipolar interactions.

Here, an attempt has been made to measure the normal modes of diffusion, as well as the adsorption and desorption kinetics of the petals in colloidal flowers using the concept proposed by Kubo [9]. Kubo generalized the concept of diffusions for situations where the particle kinetics is a superposition of random motion and directed interactions that force the particles into deterministic directions. The interactions correlate the motion of the particles that would otherwise show a degenerate individual diffusion. The correlations split the individual diffusion into statistically independent normal modes of diffusion. It is demonstrated that the adsorption and desorption kinetics as well as the mode dependence of the normal modes of petal diffusion can be understood by the competition of dipolar forces with the fluctuating forces from the viscous carrier fluid.

II. EXPERIMENT

We study the superparamagnetic Dynabeads M-270 carboxylic acid, 2.8 μm in diameter (Cat. No. 143.05 D) obtained from Invitrogen Dynal (Oslo, Norway), and Fluro-Max red fluorescent polymer microsphere beads with 1.0 μm diameter (Cat. No. R0100) obtained from Duke Scientific (Palo Alto, CA). The particles from Dynal are supplied in concentrations of approximately 2×10^9 beads ml^{-1} (10–30 mg ml^{-1}) and from Fluro-Max supplied with concentration of approximately 1% volume fraction suspended in water and respective surfactant. Paramagnetic particles are mixed with nonmagnetic particles and diluted ferrofluid EMG 705 FerroTec Ferrosound (FerroTec GmbH, Germany) with controlled proportions depending on the experiment. Electric current of 0.43 A was supplied to the water-cooled coils to produce a magnetic field of 10.0 mT, machined at University of Bayreuth. The mixture of the beads with ferrofluids was taken on a precleaned glass slide with a cover slip to reduce the air drift. Static magnetic field from the z direction was applied to the sample and was observed under the LEICA DM4000B (Leica Microsystems Wetzlar GmbH, Germany) fluorescence microscope through 63× polarization lens in reflecting mode. Videos were cap-

*thomas.fischer@uni-bayreuth.de

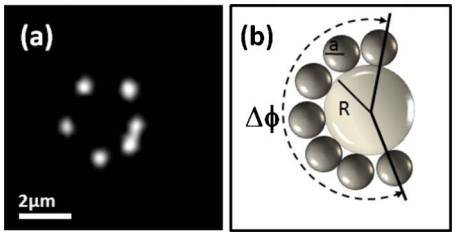

FIG. 1. (Color online) (a) Fluorescence microscope image of a six-petaled colloidal flower and (b) scheme of a colloidal flower. The paramagnetic core particle is nonfluorescent and hence not visible in the fluorescence image. The nonmagnetic fluorescence petal particles are visualized as bright spots in the fluorescence microscope image.

tured using a color charge-coupled device Basler camera (Basler A311fc) high frame rate from Basler AG, Germany.

III. ADSORPTION AND DESORPTION

Nonmagnetic beads of radius $a=0.5$ μm in a diluted aqueous ferrofluid (EMG 705 Ferrotec Ferrosound/water $=1:4$) adsorb at and desorb from the paramagnetic beads of radius $R=1.4$ μm. When they adsorb they form a colloidal flower with one paramagnetic bead at the core of the flower surrounded by several nonmagnetic beads forming the petals. A typical colloidal flower is depicted in Fig. 1. The assembly is a dynamic structure and the number of petals $N(t)$ fluctuates as a function of time because nonmagnetic beads adsorb at and desorb from the paramagnetic core. If we assume a Boltzmann distribution for the number of petals we may extract the potential energy of adsorption of N beads $U(N)$ as

$$U(N) - U(N_{\mathrm{ref}}) = -k_B T \ln\left(\frac{t(N)}{t(N_{\mathrm{ref}})}\right), \tag{1}$$

where $t(N)$ denotes the total time when one finds the colloidal flower with N petals, N_{ref} denotes a reference number of petals, and T is the temperature. In Fig. 2 we plot the adsorption potential as a function of the number of petals obtained via Eq. (1) by measuring $N(t)$ over a time duration of 4000 video frames. The adsorption potential shows a pronounced minimum near six petals. Assuming the potential to arise via dipolar attraction of the nonmagnetic beads to the paramagnetic core and due to dipolar repulsion between the equally spaced nonmagnetic petals, we predict a potential of

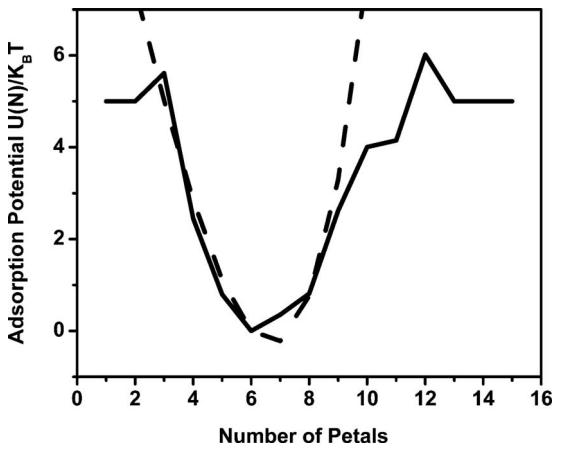

FIG. 2. Adsorption potential of the colloidal petals. The solid line is obtained from the experimental data by using Eq. (1). This potential levels off near $5k_BT$ due to lack of events. The dashed line is a fit according to Eq. (2).

$$U(N) = \frac{4\pi\mu_0\chi_F^2 H^2 a^3}{9(R/a+1)^3} N\left[-\left(\frac{\chi_p}{\chi_F}-1\right)\frac{R^3}{a^3} + \frac{1}{2}\sum_{j=1}^{N-1}\frac{1}{8\sin^3(j\pi/N)}\right]. \tag{2}$$

In Eq. (2) μ_0 denotes the vacuum permeability, χ_F and χ_p are the effective susceptibilities of the ferrofluid and of the paramagnetic particle, and H is the external magnetic field. The potential has a minimum for an equilibrium number of particles given approximately by

$$N_{eq} = \frac{2\pi}{\sqrt{3}}\sqrt{\frac{\chi_p}{\chi_F}-1}\frac{R^{3/2}}{a^{3/2}}. \tag{3}$$

The dashed line in Fig. 2 shows a fit of the experimental data (solid line) obtained from Eq. (1) to the theoretical prediction in Eq. (2) using $\chi_P=0.082$ and $\chi_F=0.063$. Note that the theoretical fit exhibits a minimum around $N=7$ instead of the value $N=6$ in the experiment.

The $2N$-dimensional conformational space of the petals is spanned by the positions $(r_j,\varphi_j, j=1,\ldots,N)$ of the petals. In an N-fold colloidal flower the equilibrium configuration is determined by the conformation $r_j=R+a$ and $\varphi_j=2\pi j/N$ $(j=1,\ldots,N)$. A transition to a $(N-1)$-fold flower happens when, for example, the Nth petal separates from the flower $(r_N\to\infty)$ and the remaining $N-1$ petals rearrange their angular positions φ_j $(j=1,\ldots,N-1)$. We describe the reaction pathway of such a conformational change by the reaction coordinate Δr. The position of the Nth petal is $r_N=R+a+\Delta r_N$, $\varphi_N=0$ and the other beads adapt the positions $r_j=R+a$, $\varphi_j=\alpha(\Delta r_N)+2[\pi-\alpha(\Delta r_N)](j-1)/(N-2)$. The angle $2\alpha(\Delta r_N)$ describes the angle between the first and the $(N-1)$th petals that readjust [from $\alpha=2\pi/N$ to $\alpha=\pi/(N-1)$], while the Nth petal leaves the flower (see top in Fig. 3). We compute the reaction pathway such that the remaining petals $j=1,\ldots,N-1$ adjust their positions to the energy minimum of the dipolar energy of the N petal system while the Nth petal is fixed at the position $r_N=R+a+\Delta r_N$. Usually no significant changes in energy are computed when the separation Δr_N of the leaving petal has exceeded $\Delta r_N>4$ μm. Hence, separations larger than 4 μm can be considered as quasi-infinite separations. In Fig. 3 we plot the dipolar energy versus the reaction coordinates Δr_N $(N=3,\ldots,11)$ for a cascade of transitions from an 11-fold colloidal flower toward a flower with two petals. The cascade from the 11-folded flower to the theoretical minimum flower with seven petals is plotted on the left side. The remaining cascade from the minimum sevenfold flower toward a two-petal flower is plotted at the right. The reaction coordinates alternate between the lower (even N) and upper

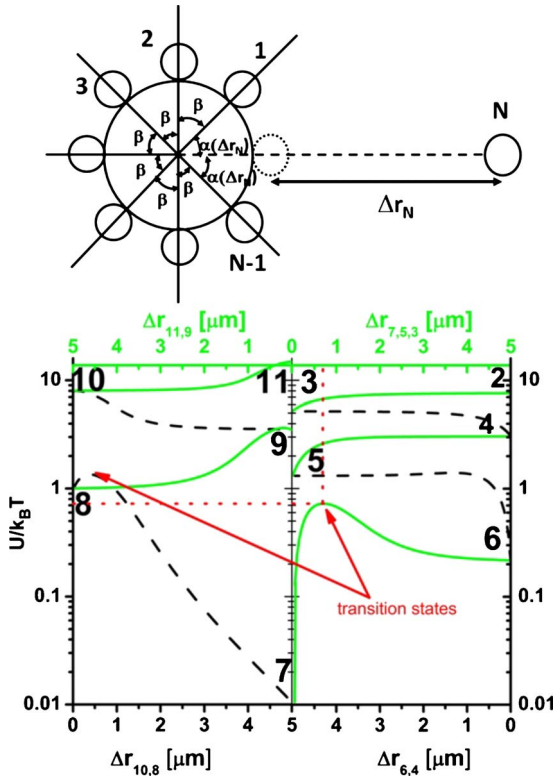

FIG. 3. (Color online) (Top) Scheme of a N-petaled flower losing the Nth petal along the reaction coordinate Δr_N, while the angular positions of the remaining petals adjust. (Bottom) The potential-energy cascade from a 11-petaled flower via the stable VII petal flower (left) toward a two-level flower (right). The flower loses the Nth petal along the reaction coordinate Δr_N; black curves correspond to the desorption of a N=even petal (lower abscissa), and green (gray) curves correspond to the desorption of a N=odd petal (upper abscissa). The energy of a petal separated by Δr_N=5 μm is indistinguishable from an infinitely separated petal and hence equals to the energy of a $(N-1)$-petaled flower. The numbers labeling the ends of the curves correspond to the number of the petals in the flower. The transition state between sixfold and sevenfold petal flowers [red (black) arrow] is at a distance of Δr=0.7 μm from the equilibrium position of the seventh petal and has an activation energy of $E_A=0.7k_BT$.

(odd N) axes. Numbers indicate equilibrium flowers of the corresponding number of petals. The potential thus changes from the N petal flower energy E_N to the $(N-1)$ petal flower energy E_{N-1}. The potential of a N petal flower with the Nth petal at a distance Δr=5 μm is indistinguishable from the potential energy of a $(N-1)$-petaled flower. This confirms that a petal at a distance $\Delta r>5$ μm can be considered as fully separated from the flower. For the desorption of the seventh petal the energy exhibits a maximum E_A along the reaction pathway. This maximum corresponds to a transition state, i.e., a saddle point in conformational space located at a distance $\Delta r_{7,max}\approx 0.7$ μm from the minimum position of the seventh petal with an activation barrier of the desorption of $(E_A-E_7)\approx 0.7k_BT$. The activation energy for the adsorption is $(E_A-E_6)\approx 0.5k_BT$. A qualitatively similar transition state is computed between the seven- and eight-petaled flowers. All other transitions in the number of petals show no transition state. Hence, all flowers with $N<6$ and $N>8$ are unstable. The six- and eight-petaled flowers are metastable $E_6, E_8>0$, and the sevenfold flower is the stable conformation $E_7=0$ for the given parameter set. Assuming an Arrhenius behavior for the rate constant $k_{6\to 7}$ of the adsorption process of the seventh petal one would expect a rate constant of the order

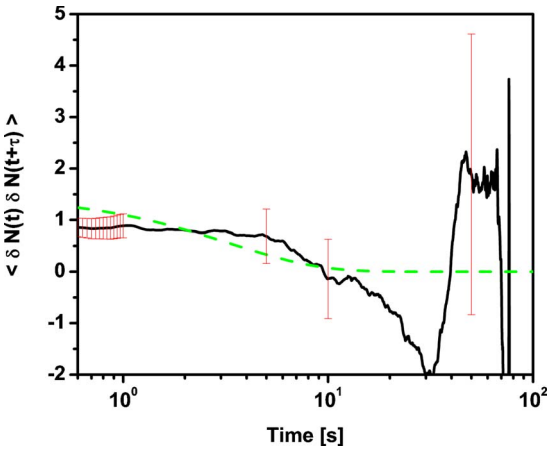

FIG. 4. (Color online) The autocorrelation function $\langle \delta N(t)\delta N(t+\tau)\rangle$ versus time as obtained from the experimental data (solid line). The number of petals changes on a time scale of 3 s. The dashed line corresponds to an exponential decay with rate constant 0.3 s^{-1}. The statistical error (error bars) of the correlation function increases when the time lag τ approaches the time of measurement $\tau_{meas}=70$ s.

$$k_{6\to 7}=\frac{k_BT}{6\pi\eta a}(\Delta r_{max})^{-2}\exp[-(E_A-E_6)/k_BT], \qquad (4)$$

where $\eta=10^{-3}$ N s m^{-2} is the ferrofluid viscosity. Inserting the values $\Delta r_{max}\approx 0.7$ μm and $(E_A-E_6)\approx 0.5k_BT$ from Fig. 3 into Eq. (4) we obtain $k_{6\to 7}\approx 0.3$ s^{-1}. In Fig. 4 we plot the autocorrelation function of the petal number,

$$\langle \delta N(t)\delta N(t+\tau)\rangle, \qquad (5)$$

where $\delta N(t)=N(t)-N_{eq}$ denotes the petal number fluctuation. The autocorrelation function decays with a typical rate of $k_{ex}\approx 0.3$ s^{-1} in good agreement with the estimate given by Eq. (4). For larger times $\tau>10$ s the experimental autocorrelation function becomes statistically unreliable since the number of events ($\propto \tau_{meas}-\tau$) drops to 1 as the time separation τ approaches the time τ_{meas} of the measurement.

IV. PETAL CONFORMATION AND DYNAMICS

Once the petals adsorb to the paramagnetic core there is some freedom of conformation, and one observes flowers with petals equally spaced around the core as well as conformations where the petals are crowded at one side of the core. We define the one-dimensional density of particles as

$$\rho=N/\Delta\phi, \qquad (6)$$

where $\Delta\phi$ denotes the minimum angular range over which the N petals are distributed and $2\pi-\Delta\phi$ is the largest gap

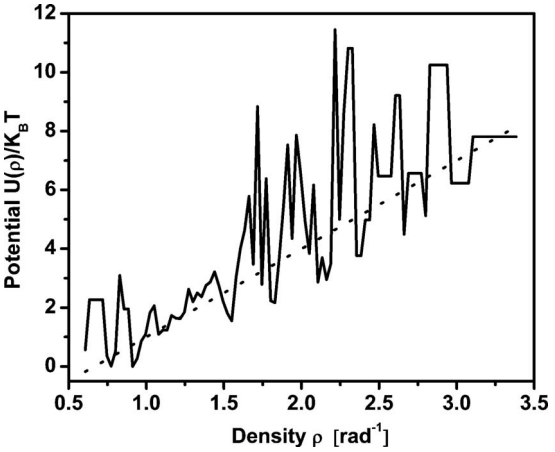

FIG. 5. Effective petal potential as a function of the petal density ρ as obtained from the experimental data via Eq. (7). The dashed line is a linear fit.

between the petals. We compute the potential energy of a conformation $U(\rho)$ as

$$U(\rho) - U(\rho_{ref}) = -k_B T \ln\left(\frac{g(\rho_{ref})\Delta\rho_{ref} t(\rho,\Delta\rho)}{g(\rho)\Delta\rho t(\rho_{ref},\Delta\rho_{ref})}\right), \quad (7)$$

where $t(\rho,\Delta\rho)$ is the total time when the petals in the flower show a density in the interval $[\rho,\rho+\Delta\rho]$ and where

$$g(\rho) \propto \left(\frac{N}{\rho} - \frac{N}{\rho_{hc}}\right)^{N-2} \quad (8)$$

is the leading-order approximation for the configurational space density [10] available for conformations of density ρ, whereas $\rho_{hc}=(R/a+1)/2$ is the maximum (hard-core) packing density of the petals around the core. Figure 5 shows the potential $U(\rho)$ computed via Eq. (7) for flowers consisting of an arbitrary number of petals. The resolution $\Delta\rho$ varies with ρ and is chosen in a way so as to ensure that $t(\rho,\Delta\rho)>0$ for all ρ. Since the data at higher potential are sparse the resolution $1/\Delta\rho$ is best at the minimum and decreases when moving toward higher potential. We find the lowest potential for densities $\rho\approx 1$ corresponding to a hexagonal arrangement of the petals with equal spacing of $\pi/3$ between the petals. The petal conformation results from the simultaneous minimization of the petal number and the minimization of the dipolar repulsion between the petals. The dipolar repulsion between the petals, however, is weak and allows for significant fluctuations around a conformation. We therefore tracked the angular position $\phi_j(t)$ $[j=1,2,3,\ldots,N(t)]$ of the adsorbed petals as a function of time. The accuracy of the tracking of $\phi_j(t)$ was better than 2°. The angular frequency $\omega_j(t)=\dot{\phi}_j(t)$ of each individual petal is a fluctuating function of time. We measure the angular frequency using finite differences of the angular positions of consecutive frames. The frame rate of the camera was 30 frames per second. We define the autocorrelation function of the angular frequency of two petals of a colloidal flower with N petals as

$$C_N(\sigma,\tau) = \langle \omega_j(t)\omega_{j\pm\sigma}(t+\tau)\delta(N(t)-N)\delta(N(t+\tau)-N)\rangle. \quad (9)$$

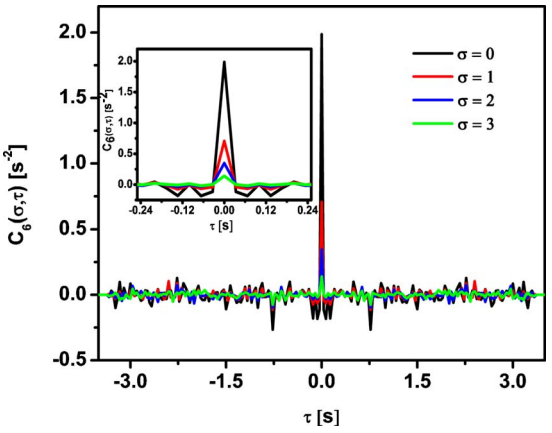

FIG. 6. (Color online) Angular frequency autocorrelation and cross-correlation functions for a colloidal flower with six petals. The black line corresponds to the autocorrelation, while the red, blue, and green lines correspond to cross correlations between nearest ($\sigma=1$), second-nearest ($\sigma=2$), and third-nearest ($\sigma=3$) neighbors, respectively.

Here, σ denotes the neighbor number ($\sigma=0$ is the same particle, $\sigma=1$ is the nearest neighbor, etc.). Both delta functions $\delta(N(t)-N)$ and $\delta(N(t+\tau)-N)$ discard all times where the petal number deviates from the fixed petal number N from the correlation.

In Fig. 6 we plot $C_6(\sigma,\tau)$ versus τ for $\sigma=0,1,2,3$. The angular frequencies are correlated for zero time delay (i.e., $\tau=0$), showing that part of the petal diffusion can be considered as a Markovian process on the time scale $\tau>0.03$ s of the measurement. The most prominent observation is that neighboring petals are not statistically independent. As does the petal autocorrelation function $C_6(0,\tau)$, the petal cross-correlation functions $C_6(\sigma\neq 0,\tau)$ also show the same albeit weaker instantaneous positive correlation. This is a dynamic proof of the deterministic interaction of the petals. Apart from this positive correlation a weak anticorrelated decay is observed for the autocorrelation $C_6(0,\tau)$ and the cross correlation $C_6(\sigma\neq 0,\tau)$ for $\tau>0.05$ s (see the inset in Fig. 6). It is a measure for the retardation of the interaction. In single file diffusion [11–13], where particles interact only via hard-core repulsion, a strong algebraic anticorrelation significantly alters the diffusion of the particles. Neighboring particles in single file diffusion remain uncorrelated at short times and become anticorrelated only at times typical for the individual diffusion time needed to encounter each other. The retardation of such a hard-core interaction is significant. Single file diffusion becomes most prominent in the thermodynamic limit $N\to\infty$, where the time scale of the simultaneous correlated diffusion of the rigid flower separates from the individual diffusion of the petals.

Our system differs from a system exhibiting single file diffusion. It has a small number of petals, and the petals interact instantaneously via the soft dipolar interactions; retardation effects are weak. In no time are the petals allowed to diffuse individually. Hence, the relatively weak delayed anticorrelation follows the instantaneous delta correlation with a relative short delay. The diffusion constant of the petals is given by half the area under the autocorrelation func-

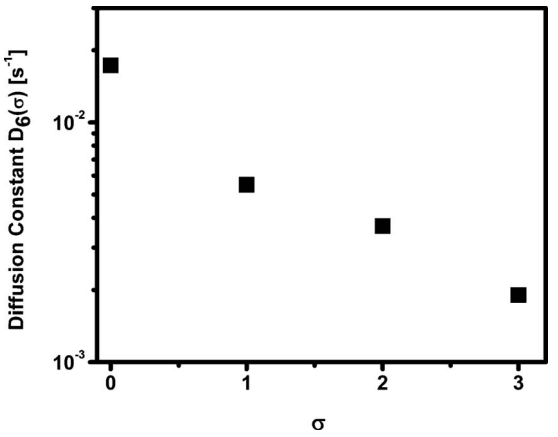

FIG. 7. Diffusion constant $D_6(\sigma)$ versus σ.

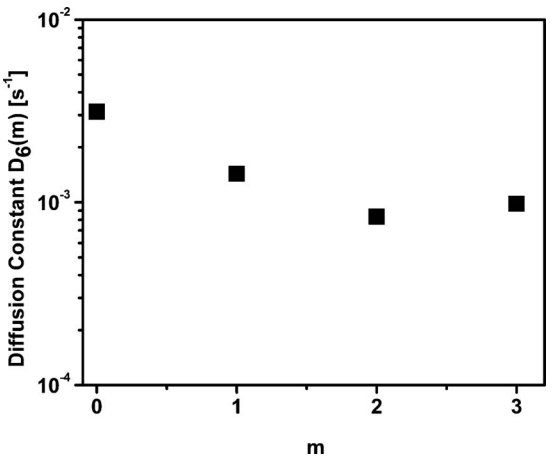

FIG. 8. Normal-mode diffusion constants $D_6(m)$ versus the mode number m.

tion. While the finite frame rate of the camera broadens the experimental correlation function, the area under the correlation function is not affected by the convolution of the data with the time resolution function of the camera. Hence, the diffusion constants have no significant dependence on the frame rate of recording,

$$D_N(\sigma) = \int_0^\infty d\tau C_N(\sigma,\tau). \tag{10}$$

Equation (10) is Kubo's [9] generalization of the concept of diffusion to particles that interact. The interaction of the particles causes the motion of one particle to statistically depend on the motion of another. The statistically dependent motion of the particles can be decomposed into statistically independent normal modes of motion. In Fig. 7 we plot the diffusion constant $D_6(\sigma)$ versus σ. The petals behave like being coupled by soft springs, with petals not diffusing independently, but with neighbors performing a correlated diffusion. The correlation decreases when moving away toward further distant neighbors. We may decompose the correlated motion of the petals into uncorrelated normal modes of diffusion via

$$\phi(m,t) = \frac{1}{\sqrt{N}} \sum_{j=1}^{N} e^{2\pi i m j/N} \phi_j(t). \tag{11}$$

The corresponding statistically independent diffusion constants of the normal modes,

$$D_N(m) = \frac{1}{N} \sum_{\sigma=1}^{N} e^{2\pi i m \sigma/N} D_N(\sigma), \tag{12}$$

are plotted in Fig. 8. The mode $m=0$ has the highest diffusion constant, and the diffusion constant decreases with the mode number m. The mode $m=0$ corresponds to a rigid rotation of all petals by the same amount. It therefore corresponds to the rotational diffusion of the entire flower that leaves the conformation of the flower unchanged. The higher modes $m>0$ involve relative motion of petals that change the conformation. Such modes are suppressed to diffuse by the dipolar repulsion between the petals. The higher is m, the shorter is the distance $2\pi/m$ between petals that are moving in opposite directions. The most likely conformation is an equilibrium conformation such that an $m \neq 0$ mode usually raises the dipolar energy of the system. This explains why the diffusion of higher modes $|m|>0$ is suppressed by the dipole-dipole interaction.

Contrary to single file diffusion the diffusion mode of the petals arises from mostly instantaneous response of the flower to conformational changes. In single file diffusion the suppression of higher modes arises from a retarded response to conformational changes that only sets in when one petal diffuses to its neighbor and encounters its hard-core repulsion.

In conclusion we have characterized the dynamic fluctuations of magnetic colloidal flowers. These fluctuations can be understood as a result of deterministic forces arising due to dipolar interactions and statistical forces arising from the collisions of the embedding fluid. The soft character of the dipolar interactions places this system between that of a free system and a system interacting via hard-core interactions. The soft confinement of the particles leads to a mode-dependent diffusion that differs from single file diffusion. The desorption and adsorption of the petals can be understood as activated processes. The colloidal flowers are thus a two-dimensional model system for the dynamics of more complex three-dimensional colloidal assemblies such as Pickering emulsions [14] and colloidosomes [15].

[1] A. van Blaaderen, R. Ruel, and P. Wiltzius, Nature (London) **385**, 321 (1997).
[2] E. R. Weeks, J. C. Crocker, A. C. Levitt, A. Schofield, and D. A. Weitz, Science **287**, 627 (2000).
[3] N. Osterman, I. Poberaj, J. Dobnikar, D. Frenkel, P. Ziherl, and D. Babic, Phys. Rev. Lett. **103**, 228301 (2009).
[4] P. Tierno, R. Muruganathan, and Th. M. Fischer, Phys. Rev. Lett. **98**, 028301 (2007).
[5] R. M. Erb, H. S. Son, B. Samanta, V. M. Rotello, and B. B. Yellen, Nature (London) **457**, 999 (2009).
[6] K. Schätzel and B. J. Ackerson, Phys. Rev. E **48**, 3766 (1993).
[7] E. Vignati, R. Piazza, and T. P. Lockhart, Langmuir **19**, 6650 (2003).
[8] Y. Terada and M. Tokuyama, J. Phys. Soc. Jpn. **79**, 034802 (2010).
[9] R. Kubo, J. Phys. Soc. Jpn. **12**, 570 (1957).
[10] The assumption that $2\pi-\Delta\phi$ is the largest gap forbids conformations with density ρ that have a larger gap between the first and Nth petals. Three particle correlations of this kind have been neglected when approximating the conformational space density $g(\rho)$. The systematic error introduced in this way cancels near the potential minimum due to the normalization with $g(\rho_{ref})$.
[11] Q. H. Wei, C. Bechinger, and P. Leiderer, Science **287**, 625 (2000).
[12] J. Kärger, Phys. Rev. A **45**, 4173 (1992).
[13] V. Kukla, J. Kornatowski, D. Demuth, I. Gimus, H. Pfeifer, L. V. C. Rees, S. Schunk, K. K. Unger, and J. Kärger, Science **272**, 702 (1996).
[14] R. Aveyard, B. P. Binks, and J. H. Clint, Adv. Colloid Interface Sci. **100-102**, 503 (2003).
[15] A. D. Dinsmore, M. F. Hsu, M. G. Nikolaides, M. Marquez, A. R. Bausch, and D. A. Weitz, Science **298**, 1006 (2002).